Atomically defined mechanism for proton transfer to a buried redox centre in a protein

Kaisheng Chen*†, Judy Hirst†‡§, Raul Camba†‡, Christopher A. Bonagura*, C. David Stout‖, Barbara. K. Burgess* & Fraser A. Armstrong‡

** Department of Molecular Biology and Biochemistry, University of California, Irvine, California 92612, USA*
‡ Department of Chemistry, Oxford University, Oxford OX1 3QR, UK
‖ Department of Molecular Biology, The Scripps Research Institute, 10550 North Torrey Pines Road, La Jolla, California 92037-1083, USA
† These authors contributed equally to this work
§ Present address: Medical Research Council Dunn Human Nutrition Unit, Hills Road, Cambridge CB2 2XY, UK

The basis of the chemiosmotic theory is that energy from light or respiration is used to generate a trans-membrane proton gradient[1]. This is largely achieved by membrane-spanning enzymes known as 'proton pumps'[2–5]. There is intense interest in experiments which reveal, at the molecular level, how protons are drawn through proteins[6–13].Here we report the mechanism, at atomic resolution, for a single long-range electron-coupled proton transfer. In *Azotobacter vinelandii* ferredoxin I, reduction of a buried iron–sulphur cluster draws in a solvent proton, whereas re-oxidation is 'gated' by proton release to the solvent. Studies of this 'proton-transferring module' by fast-scan protein film voltammetry, high-resolution crystallography, site-directed mutagenesis and molecular dynamics, reveal that proton transfer is exquisitely sensitive to the position and pK of a single amino acid. The proton is delivered through the protein matrix by rapid penetrative excursions of the side-chain carboxylate of a surface residue (Asp 15), whose pK shifts in response to the electrostatic charge on the iron–sulphur cluster. Our analysis defines the structural, dynamic and energetic requirements for proton courier groups in redox-driven proton-pumping enzymes.

Current studies of proton-pumping enzymes such as bacteriorhodopsin and cytochrome *c* oxidase are revealing the existence of 'proton wires' comprising chains of water molecules and protonatable amino-acid side-chains[2–12]. Apart from water channels, which provide natural proton conductors[14], transfer of protons is heavily restricted by their short tunnelling distance; thus, whereas electrons may easily tunnel 10 Å, a proton with comparable energy is limited to hops of less than 0.25 Å[15–17]. This restriction can be used, along with barriers imposed by pK differences between proton donors and acceptors[18], to control proton flow in response to electron-transfer events at nearby redox sites[2–12]. However, proton pumps are complex membrane-bound enzymes and mechanistic details are difficult to analyse coherently. We now report conclusive studies of the mechanism of redox-driven proton transfer between solvent and a buried iron–sulphur cluster ([3Fe–4S]) in ferredoxin I (FdI) from *A. vinelandii*. This small protein provides an electron/proton-transfer 'module' with which to understand the redox-linked proton-transferring components of the larger enzymes[13,19]. A major advantage of the FdI system is that native and mutant structures are known to high structural resolution in all

Box 1

Sequential electron and proton transfers at the [3fe–45] cluster in ferredoxin I

Scheme I, Sequence of electron and proton transfers defining the redox chemistry of the [3Fe–4S] cluster in Ferredoxin I. Electron transfers (standard first-order electrochemical rate constant, k_0) are fast, and E_{alk} is the reduction potential if pH ≫ $pK_{cluster}$.

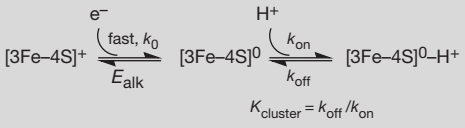

Scheme II, Sequence by which proton transfer to the cluster is catalysed by Asp 15 (B). Fast proton transfer (species highlighted in blue) is pH dependent, and protonation constants of Asp 15 are sensitive to cluster charge. At low pH, Asp 15 re-protonates (K_2), thus inhibiting proton transfer off the cluster. For native *A. vinelandii* FdI, pK_{OX} = 5.4. See Table I for rate expressions.

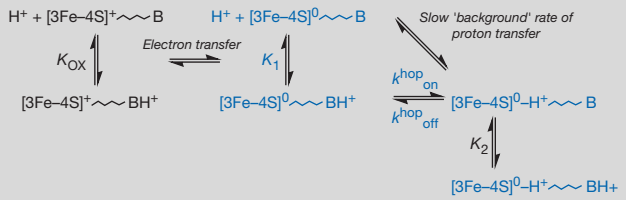

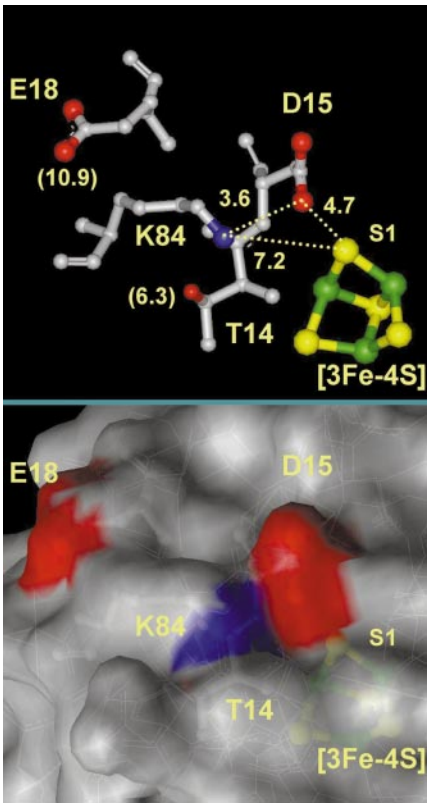

Figure 1 The residues in the vicinity of the [3Fe–4S] cluster in oxidized native *Azotobacter vinelandii* Ferredoxin I, taken from coordinates 7FD1. The upper frame shows the side chains of residues that were varied in this study, and indicates the separation (in Å) between D15 $O\delta_1$ and S1, the least buried μ_2 sulphide of [3Fe–4S]. Only the major conformation of the K84 side chain is shown (68% occupancy). The lower frame shows the same view, onto which is superimposed the solvent-accessible surface (calculated with a 1.4 Å probe). The carboxylate Oδ atoms of D15 and E18, and Nζ of K84 are solvent exposed. The Lys 84 side chain adopts two conformations in the oxidized native protein, as shown by the pH 8.5 structure (Protein data bank (PDB) code 7FD1, ref. 22) where these have 68% and 32% relative occupancies and (K84)Nζ–(D15)$O\delta_1$ distances of 3.6 Å and 3.1 Å respectively. The Glu 18 side chain is disordered (anomalously high B values).

relevant oxidation and protonation states[20–22]. Importantly, FdI can be studied by fast-scan protein film voltammetry, a technique able to reveal, in detail, the bi-directional kinetics of coupled proton–electron-transfer reactions and their relation to thermodynamics[13,23] (See Supplementary Information).

Scheme I (Box 1) shows the bi-directional proton transfer that accompanies fast electron transfer to the $[3Fe–4S]^{1+/0}$ cluster of FdI. Reduction drives a proton onto the cluster (k_{on}), while its reoxidation is 'gated' by proton release (k_{off}). Scheme I stems from numerous lines of evidence. The $[3Fe–4S]^{1+/0}$ reduction potential is pH-dependent, and one proton is taken up in the reduced state ($pK_{cluster} = 7.8$)[13,23]. This uptake can be observed spectroscopically: thus, circular dichroism and magnetic circular dichroism spectra of oxidized FdI (spin-state (S) = 1/2) are independent of pH, whereas the one-electron reduced FdI ($[3Fe–4S]^{0}$, S = 2) shows an acid–base transition[24]. The X-ray structures of oxidized and reduced FdI at high and low pH eliminate the possibility that the pH-dependent spectral changes are due to ligand exchange and/or structural rearrangements[20]. Site-directed mutagenesis has established that the spectral changes are not due to protonation of the nearest ionizable residue (Asp 15)[19], while Mössbauer spectroscopy has revealed that protonation perturbs the electronic structure of the cluster[25]. The obvious protonation site is a μ_2 sulphide (one of the three cluster sulphur atoms with a free coordination site).

Figure 1 shows the region above the buried [3Fe–4S] cluster, both within the protein and looking down on the surface. Even at highest resolution (1.4 Å), the crystal structures, and NMR on a related protein[26], reveal no internal water molecules (or accommodating spaces) to act as proton-transfer agents[14,20–22]. The starting point for this study is the mutant (D15N) in which Asp 15, the closest ionizable residue, which moves upon cluster reduction[20], is changed to Asn[19]. Protein film voltammetry showed that proton coupling is severely retarded in D15N FdI, indicating that the carboxylate acts as a proton relay group[13,19]. However, in the native protein, Asp 15 is salt-bridged to Lys 84, raising the possibility of proton migration across the bridge. In addition, the highly mobile side chain of a second surface carboxylate residue, Glu 18, lies close by.

With the ability to make extensive kinetic, thermodynamic and structural measurements, we designed several new mutants. Figure 2 shows the arrangements of cluster-region amino acids for all variants, with distances between relevant atoms and the μ_2 sulphide (S1) situated closest to the protein surface. Circular dichroism spectroscopy confirmed that protonation of $[3Fe—4S]^{0}$ occurs in all cases. Table 1 displays the corresponding kinetic and

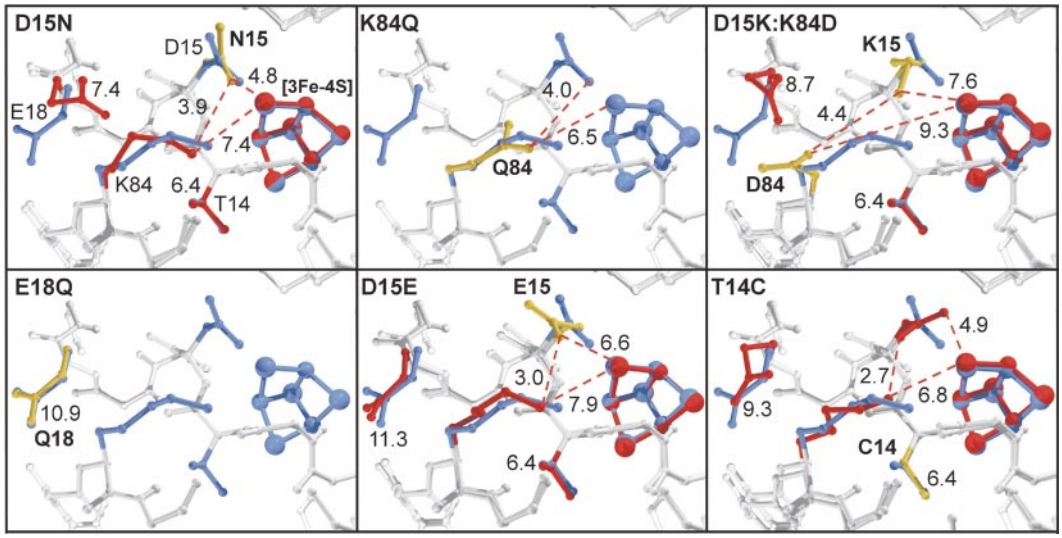

Figure 2 Structures of the various mutant forms of FdI in the region of interest, compared with the structure of oxidized native FdI. Side chains for the native protein are shown in blue and those altered by mutagenesis in yellow. Where X-ray structures are available, the positions of the other residues in the mutant proteins are shown in red. All distances are given in ångstroms and where lines are not shown the number refers to the distance between the indicated residue and S1. Structures have been solved for D15N (PDB code 1FDD, ref. 19), D15K/K84D (PDB code 1B0T), D15E (PDB code 1D3W) and T14C (PDB code 1A6L, ref. 27). Crystals have not been obtained for K84Q or E18Q: these structures were modelled using the Insight II/Biopolymer program from Molecular Simulations for which the native oxidized structure (1.35 Å, PDB code 7FD1) was substituted with the desired mutant residue at the program-assigned minimum energy orientation.

Table 1 Kinetic and thermodynamic parameters for 'on' and 'off' proton transfers

Fast	E_{alk} (V)	$pK_{cluster}$ (high pH)	$pK_{cluster}$ (low pH)	$k_{on}(M^{-1}s^{-1})$* (pH 7.0)	$k_{off}(s^{-1})$* (pH 7.0)	pK_1	pK_2	$k_{on}^{hop}(s^{-1})$	$k_{off}^{hop}(s^{-1})$
Native	–0.443	7.8 ± 0.1	6.5 ± 0.1	7.9×10^9	308	7.2 ± 0.1	5.9 ± 0.1	1,294 ± 100	332 ± 25
E18Q	–0.453	7.7 ± 0.1	6.7 ± 0.1	4.8×10^9	207	7.1 ± 0.1	6.1 ± 0.1	930 ± 90	230 ± 25
T14C	–0.464	8.4 ± 0.1	7.1 ± 0.1	6.6×10^9	207	8.0 ± 0.1	6.7 ± 0.1	720 ± 70	310 ± 25
K84Q	–0.476	8.1 ± 0.1	6.6 ± 0.1	9.0×10^9	232	7.4 ± 0.1	5.9 ± 0.1	1,252 ± 100	250 ± 25
Native (D_2O)	–0.443	7.8 ± 0.1	6.5 ± 0.1	6.0×10^9	222	7.2 ± 0.1	5.9 ± 0.1	970 ± 100	240 ± 25
Slow	E_{alk} (V)	$pK_{cluster}$		$k_{on}(M^{-1}s^{-1})$	$k_{off}(s^{-1})$				
D15N	–0.408	6.9 ± 0.1		2.0×10^7	2.5 ± 0.1				
D15K–K84D	–0.397	6.6 ± 0.1		1.2×10^7	3.0 ± 0.1				
D15E	–0.388	6.7 ± 0.1		2.0×10^7	4.5 ± 0.2				

All terms are as defined in Schemes I and II.
*For the fast reactions, interpreted in terms of Scheme II, $k_{on} = k_{on}^{hop}/([H^+] + K_1)$ and $k_{off} = k_{off}^{hop}K_2/([H^+] + K_2)$. Agreement with the simple bimolecular rate law of Scheme I requires consideration of the fact that interaction with Asp 15 causes the pK of the cluster to differ at high and low pH. In all cases k_0, the standard first-order electrochemical rate constant for electron exchange at the reduction potential, is $> 200\,s^{-1}$; the exponential increase in rate that occurs as a driving force is applied means that electron transfer is never rate limiting.

thermodynamic parameters for 'on' and 'off' proton transfers, defined according to Schemes I and II (Box 1), and measured by protein film cyclic voltammetry. In all cases, reduction involves electron transfer followed by proton transfer, whereas oxidation requires that proton transfer precede electron transfer, that is, the two processes do not occur in concert. Electron transfer is very fast and is clearly separated from proton transfer.

The mutants fall sharply into two categories with respect to proton-transfer kinetics—'slow' and 'fast'—with rates differing by three orders of magnitude. The kinetics of the 'slow' mutants are simple and pH-independent (they are described adequately by Scheme I) and rates are similar in each case. By contrast, the 'fast' mutants show a complex pH dependence (Scheme II) with second-order 'on' rate constants approaching diffusion control at pH 7.

Referring to Fig. 2, the following facts are established. The D15N mutation replaces the carboxylate by carbamide and the slow proton-transfer rate is consistent with loss of a protonatable group (base B) which acts as a proton relay (Scheme II)[13,19]. However, the mutation also disrupts the salt bridge between the Asp 15 carboxylate and a surface lysine (Lys 84)[19]. In addition, the side chain of Glu 18 shifts, although the change is less-defined due to disorder. In the mutant K84Q, Lys 84 is changed to a residue (Gln) that cannot form a salt-bridge to Asp 15. The fast proton-transfer kinetics demonstrate that it is the presence of the carboxylate and not the salt-bridge that is important. The double mutant D15K/K84D was designed to invert the salt-bridge orientation; however, the salt-bridge does not form. Proton transfer is slow, as it is in D15N, showing that the introduced Asp 84 side chain is incorrectly placed to function as a proton-transfer group and that lysine cannot substitute for aspartate at position 15. The possibility that Glu 18 facilitates proton transfer was eliminated by the mutant E18Q, which has very similar rates to the native protein. Experiments with D15E finally established the critical nature of the distance between the cluster and the carboxylate at position 15. Insertion of a single CH_2 group in the side chain (which increases the distance by approximately 2 Å) retards proton transfer as much as deletion of the carboxylate altogether (Table I). The T14C mutant has a polarizable S atom within the sphere of influence of the cluster and raises the cluster pK while the position of the carboxylate is not significantly changed[27]. The native proton-transfer kinetics are retained, confirming that they are dependent solely on the position of the carboxylate.

The exacting requirement for Asp 15 is thus demonstrated, leading to a detailed model for the mechanism of proton transfer between water at the protein surface and the buried redox centre. The data in Table 1 show that the H_2O/D_2O isotope effect for the native protein is small (approximately 1.3), and reveal (from the interdependence of respective pK values) that there are significant electrostatic interactions between the cluster and Asp 15. As shown in Fig. 3a, electron transfer drives rotation of the Asp 15 carboxylate about the Cβ–Cγ bond and increases the Oδ to S1 distance from 4.7 Å to 4.9 Å, in accordance with the less favourable electrostatics[22]. More significantly, the pK of the carboxylate increases to 7.2 compared with 5.4 in the oxidized ($[3Fe–4S]^{1+}$) state (pK_{OX} in Scheme II), thus promoting proton capture from solvent water[18]. It is important to note that a sizeable, transient shift in pK value is essential for fitting the data. After the proton has transferred to the cluster, the pK drops back to 5.9, and the X-ray structure of the reduced protein at pH 6.1 reveals that the Asp 15 carboxylate reverts towards its position in the oxidized form[20]. This 'relaxation' is expected because the $[3Fe–4S]^0$-H^+ cluster has the same electrical charge as the oxidized $[3Fe–4S]^{1+}$ cluster.

To explain how Asp 15 mediates such fast proton transfer, it is necessary to ascertain whether a proton that has transferred from solvent to a carboxylate O atom can then be carried easily to within hydrogen-bonding distance of the cluster S1 atom[28]. We therefore carried out molecular dynamics calculations to study the mobility of the state in which the reduced cluster is unprotonated while Asp 15 is protonated and thus no longer repelled by the increased negative charge on the cluster. The results reveal that the Asp 15 side chain is very mobile, executing a high frequency of short-range encounters between Oδ and S1 atoms (Fig. 3b). Thus, within 80 ps, an Oδ atom makes one excursion to 3.05 Å (Fig. 3c), well within the sum of van der Waals radii, and five other excursions to distances less than 4 Å. The motions of the side-chain carboxyl/carboxylate group thus convey H^+ between solvent and reduced cluster, accomplishing 'atom-to-atom' transfer across this hydrophobic barrier. Cluster deprotonation occurs by reversal of these steps, noting that at pH < 5.9, protonation of Asp 15 inhibits proton transfer off the cluster.

In conclusion, fast proton transfer in FdI requires the presence of Asp 15 and rapid penetrative excursions of its side-chain carboxyl/carboxylate to within hydrogen-bonding distance of the cluster. Our experiments, which combine detailed kinetic and thermodynamic data for a series of mutants with molecular dynamics based on high-resolution protein crystal structures, highlight the exacting specifications that must be met for proton-pumping motifs in enzymes[2–5]. The pK values of the proton-relaying carboxylate and the buried active site are tightly coupled and adjust to facilitate sequential transfers of an electron and a proton. Re-oxidation is gated by

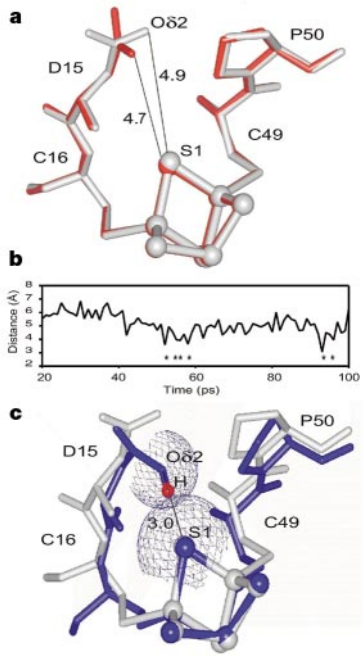

Figure 3 Movement of the Asp15 side chain during redox-driven proton transfers. **a**, Comparison of oxidized (red; PDB code 7FD1) and reduced (grey; PDB code 7FDR) high-pH structures of native FdI in the region of the cluster and Asp 15. Upon reduction, the Lys 84 side chain adopts a single conformation with a Nζ–$Oδ_1$ distance of 3.3 Å, and the carboxylate side chain has rotated by 90°. (In accordance with previous nomenclature, the closest O atom to the cluster in the reduced form is denoted $Oδ_2$, whereas it is $Oδ_1$ in the oxidized form[22].) **b**, Distances of $Oδ_2$ (from Asp 15) to S1 (from the cluster) during the molecular dynamics simulation; asterisks indicate the points where the distance is below 4 Å. **c**, Superposition of the reduced native FdI (grey) structure (also shown in **a**) and one of the molecular-dynamics-generated snapshot structures (blue) around the region of Asp 15, showing one of the approaches of $Oδ_2$ to the S1 atom of $[3Fe–4S]^0$ within the period of simulation. The distance between $Oδ_2$ and S1 is 4.9 Å for the native structure and 3.0 Å for the molecular-dynamics-generated structure. The H atom is positioned collinear with $Oδ_2$–S1 at a normal bond distance (1.0 Å) from $Oδ_2$. Van der Waals surfaces of $Oδ_2$ (radius 1.4 Å) and S1 (1.85 Å) are shown. For this closest approach, Oδ and S1 are well within the sum (1.4 + 1.85 = 3.25 Å) of their van der Waals radii and, in the limit of a collinear O–H···S arrangement, the resulting H–S distance is approximately 2.25 Å.

proton transfer, demonstrating how biology can control long-range electron transfer by linking it to a far more discriminating process. Mechanistic requirements for proton transfer are so stringent that even minor structural changes produce decreases in rate over orders of magnitude. □

Methods

Protein film voltammetry

Protein film voltammetry probes electron-transfer processes that are induced by perturbing the electrochemical potential applied to a mono-/submono-layer of protein molecules bound at an electrode surface (See Supplementary Information). Electron transfers in and out of the active site are observed as electrical current signals, which are altered in specific ways if there is coupling to processes such as proton transfer. Thus, by analysing signals over a range of voltage scan rate and pH, a detailed and integrated picture of the coupling kinetics and energetics is obtained. All measurements were carried out as described previously[13] and 'trumpet plots' of peak positions versus scan rate were analysed in terms of the kinetics and thermodynamics described by Scheme II.

Site directed mutagenesis and protein crystallography

Site directed mutagenesis and protein purification were carried out as previously reported[19,27]. Crystal structures were determined accordingly to procedures recently described[22].

Molecular dynamics

Molecular dynamics simulations were carried out using the DISCOVER program from Molecular Simulations. The AMBER force field used for the protein and Fe–S cluster was as described[29] except that cluster atomic charges were derived from Xα density functional calculations[30]. The structure of reduced FdI at pH 8.5 (1.35 Å resolution, protein data bank code 7FDR, ref. 21) was used as the starting model except that the $O\delta_2$ atom of Asp 15 was protonated. Besides the crystallographic water molecules, a 9 Å layer of water molecules was added around the protein and those occupying the outermost 5 Å were constrained to prevent their evaporation. After initial minimization, the system was heated for 5 ps at 100, 200, 273 K, and then the dynamics were run at 273 K for 100 ps with a time step of 1.5 fs: the first 20 ps were discarded. The mean structure over the 80 ps considered had r.m.s. deviation values from the starting structure of 1.20 Å for the backbone atoms and 1.45 Å for all heavy atoms. The individual structures generated had average r.m.s. deviation values (from the mean structure) of 0.68 Å for the backbone atoms and 0.86 Å for all heavy atoms, within the range expected[26].

Received 26 November 1999; accepted 12 April 2000.

1. Nicholls, D. G. & Ferguson, S. J. Bioenergetics 2 (Academic, San Diego, 1992).
2. Wikström, M. Proton translocation by bacteriorhodopsin and heme-copper oxidases. *Curr. Opin. Struct. Biol.* **8,** 480–488 (1998).
3. Gennis, R. B. How does cytochrome oxidase pump protons? *Proc. Natl Acad. Sci. USA* **95,** 12747–12749 (1998).
4. Malmström, B. G. Cytochrome oxidase: pathways for electron tunneling and proton transfer. *J. Biol. Inorg. Chem.* **3,** 339–343 (1998).
5. Michel, H. The mechanism of proton pumping by cytochrome *c* oxidase. *Proc. Natl Acad. Sci. USA* **95,** 12819–12824 (1998).
6. Rammelsberg, R., Huhn, G., Lübben, M. & Gerwert, K. Bacteriorhodopsin's intramolecular proton-release pathway consists of a hydrogen-bonded network. *Biochemistry* **37,** 5001–5009 (1998).
7. Luecke, H., Schobert, B., Richter, H.-T., Cartailler, J. P. & Lanyi, J. Structural changes in bacteriorhodopsin during ion transport at 2 Å resolution. *Science* **286,** 255–260 (1999).
8. Nabedryk, E., Breton, J., Okamura, M. Y. & Paddock, M. L. Proton uptake by carboxylic acid groups upon photoreduction of the secondary quinone (Q_B) in bacterial reaction centres from Rhodobacter sphaeroides: FTIR studies on the effects of replacing Glu H173. *Biochemistry* **37,** 14457–14462 (1998).
9. Yoshikawa, S. *et al.* Redox-coupled crystal structural changes in bovine heart cytochrome *c* oxidase. *Science* **280,** 1723–1729 (1998).
10. Konstantinov, A. A., Siletsky, S., Mitchell, D., Kaulen, A. & Gennis, R. B. The roles of two proton input channels in cytochrome c oxidase from *Rhodobacter sphaeroides* probed by the effects of site-directed mutations on time-resolved electrogenic intraprotein proton transfer. *Proc. Natl Acad. Sci. USA* **94,** 9085–9090 (1997).
11. Lübben, M., Prutsch, A., Mamat, B. & Gerwert, K. Electron transfer induces side-chain conformational changes of glutamate-286 from cytochrome bo_3. *Biochemistry* **38,** 2048–2056 (1999).
12. Junemann, S., Meunier, B., Fisher, N. & Rich, P. R. Effects of mutation of the conserved glutamic acid-286 in subunit I of cytochrome *c* oxidase from *Rhodobacter sphaeroides*. *Biochemistry* **38,** 5248–5255 (1999).
13. Hirst, J. *et al.* Kinetics and mechanism of redox-coupled, long-range proton transfer in an iron-sulfur protein. Investigation by fast-scan protein-film voltammetry. *J. Am. Chem. Soc.* **120,** 7085–7094 (1998).
14. Meyer, E. Internal water molecules and H-bonding in biological macromolecules: a review of structural features with functional implications. *Protein Sci.* **1,** 1543–1562 (1992).
15. Beratan, D. N., Onuchic, J. N., Winkler, J. R. & Gray, H. B. Electron-tunneling pathways in proteins. *Science* **258,** 1740–1741 (1992).
16. Page, C. G., Moser, C. C., Chen, X. & Dutton, P. L. Natural engineering principles of electron tunnelling in biological oxidation-reduction. *Nature* **402,** 47–52 (1999).
17. Klinman, J. P. Quantum mechanical effects in enzyme-catalyzed hydrogen transfer reactions. *Trends Biochem. Sci.* **14,** 368–373 (1989).
18. Gutman, M. & Nachliel, E. The dynamics of proton exchange between bulk and surface groups. *Biochim. Biophys. Acta* **1231,** 123–138 (1995).
19. Shen, B. *et al.* *Azotobacter vinelandii* ferredoxin I. Aspartate 15 facilitates proton transfer to the reduced [3Fe–4S] cluster. *J. Biol. Chem.* **268,** 25928–25939 (1993).
20. Stout, C. D. Crystal structures of oxidized and reduced *Azotobacter vinelandii* ferredoxin at pH 8 and 6. *J. Biol. Chem.* **268,** 25920–25927 (1993).
21. Stout, C. D., Stura, E. A. & McRee, D. E. Structure of Azotobacter vinelandii 7Fe ferredoxin at 1. 35 Å resolution and determination of the [Fe–S] bonds with 0. 01 Å accuracy. *J. Mol. Biol.* **278,** 629–639 (1998).
22. Schipke, C. G., Goodin, D. B., McRee, D. E. & Stout, C. D. Oxidized and reduced *Azotobacter vinelandii* ferredoxin I at 1. 4 Å resolution: conformational change of surface residues without significant change in the $[3Fe–4S]^{+/0}$ cluster. *Biochemistry* **38,** 8228–8239 (1999).
23. Armstrong, F. A., Heering, H. A. & Hirst, J. Reactions of complex metalloproteins studied by protein-film voltammetry. *Chem. Soc. Rev.* **26,** 169–179 (1997).
24. Stephens, P. J. *et al.* Circular-dichroism and magnetic circular-dichroism of *Azotobacter vinelandii* ferredoxin I. *Biochemistry* **30,** 3200–3209 (1991).
25. Hu, Z. G., Jollie, D., Burgess, B. K., Stephens, P. J. & Münck, E. Mössbauer and EPR studies of *Azotobacter vinelandii* ferredoxin I. *Biochemistry* **33,** 14475–14485 (1994).
26. Aono, S. *et al.* Solution structure of oxidized Fe_7S_8 ferredoxin from the thermophillic bacterium *Bacillus schlegelii* by ^{1}H NMR spectroscopy. *Biochemistry* **37,** 9812–9826 (1998).
27. Gao-Sheridan, A T14C variant of *Azotobacter vinelandii* ferredoxin I undergoes facile $[3Fe–4S]^0$ to $[4Fe–4S]^{2+}$ conversion in vitro but not *in vivo*. *J. Chem. Biol.* **273,** 33692–33701 (1998).
28. Guthrie, J. P. Intrinsic barriers for protons transfer reactions involving electronegative atoms, and the water mediated proton switch: an analysis in terms of Marcus theory. *J. Am. Chem. Soc.* **118,** 12886–12890 (1996).
29. Banci, L., Bertini, I., Carloni, P., Luchinat, C. & Orioli, P. L. Molecular-dynamics on HIPIP from *Chromatium vinosum* and comparison with NMR data. *J. Am. Chem. Soc.* **114,** 10683–10689 (1992).
30. Noodleman, L., Norman, J. G. Jr, Osborne, J. H., Aizman, A. & Case, D. A. Models for ferredoxins—electronic structures of iron sulfur clusters with one, two and four iron atoms. *J. Am. Chem. Soc.* **107,** 3418–3426 (1985).

Supplementary information is available on *Nature*'s World-Wide Web site (http://www.nature.com) or as paper copy from the London editorial office of *Nature*.

Acknowledgements

We thank T. Poulos and J. Lanyi for comments on the manuscript. This research was supported by grants from the NIH, EPSRC, and BBRSC. B.B.K. thanks The Fulbright Commission for a Senior Scholarship, and the John Simon Guggenheim Foundation for a Travelling Fellowship. R.C. is grateful to The National Council of Science and Technology of Mexico (CONACYT) for their support.

Correspondence and requests for materials should be addressed to F.A.A. (e-mail: fraser.armstrong@chem.ox.ac.uk).